

## The Donor of the Black-Hole X-Ray Binary MAXI J1820+070

JOANNA MIKOŁAJEWSKA,<sup>1</sup> ANDRZEJ A. ZDZIARSKI,<sup>1</sup> JANUSZ ZIÓŁKOWSKI,<sup>1</sup> MANUEL A. P. TORRES,<sup>2,3</sup> AND JORGE CASARES<sup>2,3</sup>

<sup>1</sup>*Nicolaus Copernicus Astronomical Center, Polish Academy of Sciences, Bartycka 18, PL-00-716 Warszawa, Poland*

<sup>2</sup>*Instituto de Astrofísica de Canarias, E-38205 La Laguna, Tenerife, Spain*

<sup>3</sup>*Departamento de Astrofísica, Universidad de La Laguna, E-38206 La Laguna, Tenerife, Spain*

### ABSTRACT

We estimate the parameters of the donor of the accreting black-hole binary MAXI J1820+070. The measured values of the binary period, rotational and radial velocities and constraints on the orbital inclination imply the donor is a subgiant with the mass of  $M_2 \approx 0.49_{-0.10}^{+0.10} M_\odot$  and the radius of  $R_2 \approx 1.19_{-0.08}^{+0.08} R_\odot$ . We re-analyze the previously obtained optical spectrum from the Gran Telescopio Canarias, and found it yields a strict lower limit on the effective temperature of  $T > 4200$  K. We compile optical and infrared fluxes observed during the quiescence of this system. From the minima  $r$  and  $i$ -band fluxes found in Pan-STARSS1 Data Release 2 pre-discovery imaging and for a distance of  $D \approx 3$  kpc, reddening of  $E(B-V) = 0.23$  and  $R_2 \approx 1.11 R_\odot$ , we find  $T \lesssim 4230$  K, very close to the above lower limit. For a larger distance, the temperature can be higher, up to about 4500 K (corresponding to a K5 spectral type, preferred by previous studies) at  $D = 3.5$  kpc, allowed by the Gaia parallax. We perform evolutionary calculations for the binary system and compare them to the observational constraints. Our model fitting the above temperature and radius constraints at  $D \approx 3$  kpc has the mass of  $0.4 M_\odot$ ,  $T \approx 4200$  K and solar metallicity. Two alternative models require  $D \gtrsim 3.3$ – $3.4$  kpc at  $0.4 M_\odot$ ,  $T \approx 4500$  K and half solar metallicity, and  $0.5 M_\odot$ ,  $T \approx 4300$  K and solar metallicity. These models yield mass transfer rates of  $\sim 10^{-10} M_\odot/\text{yr}$ , compatible with those based on the estimated accreted mass of  $\approx 2 \times 10^{25}$  g and the time between the 2018 discovery and the 1934 historical outburst.

### 1. INTRODUCTION

The outburst of the transient accreting low-mass X-ray binary (LMXB) MAXI J1820+070 was discovered on 2018-03-06 in the optical range with the  $V$ -band magnitude of 14.88 (Tucker et al. 2018). It was detected in X-rays six days later (on 2018-03-11; Kawamuro et al. 2018). Given the high observed brightness and long duration of the outburst, it was the subject of a large number of observing campaigns, whose results have led to numerous insights into the nature of this source. Torres et al. (2019, 2020) have unambiguously determined that the accretor is a black hole (BH). However, the donor parameters have remained relatively loosely constrained (see Sections 2.1–2.3). More accurate determinations of the donor radius and temperature are important for modelling the emission of the accretion flow in the quiescent state of this system (Poutanen et al. 2022). Also, the metallicity of MAXI J1820+070 is of importance for calculation of the inner radius of the accretion disk during the outburst. On one hand, Buisson et al. (2019) found the Fe abundance to be higher than solar by a factor of  $\approx 3$ – $9$  and the disk extending close to the innermost stable circular orbit from fitting reflection model spectra to X-ray data in the luminous hard state. On the other, fits by Zdziarski et al. (2021) obtained a fractional Fe abundance of  $\approx 1.1$ – $1.6$  and a truncated disk. However, Fe abundances from spectral fits are subject to significant systematic errors related to the effects of the assumed density of the reflector (García et al. 2018). Therefore, an independent estimate of the abundances of the donor

would be highly valuable in constraining the results of X-ray spectroscopy.

In this work, we consider evolutionary models of the binary, with the goal of constraining better the mass and radius of the stellar companion as well as its spectral type and metallicity. In Section 2.1, we review available constraints on the distance and binary parameters, in Section 2.2, we compile available mid-infrared to ultraviolet photometric measurements, which constrain the radius and temperature of the donor, in Section 2.3, we consider its metallicity, in Section 2.4, we estimate the average mass accretion rate, and in Section 3, we perform the evolutionary calculations. Section 4 provides a summary of our results.

### 2. SYSTEM PARAMETERS

#### 2.1. The distance and binary parameters

MAXI J1820+070 is relatively nearby, with a distance of  $D \approx 2.96 \pm 0.33$  kpc measured based on a radio parallax (Atri et al. 2020). This agrees well with the current Gaia EDR3 parallax measurement of  $D = 2.81_{-0.39}^{+0.70}$  kpc (Bailer-Jones et al. 2021). Then, Wood et al. (2021) determined  $D \leq 3.11 \pm 0.06$  kpc based on the proper motion of two moving transient ejecta (Mirabel & Rodríguez 1994) during the hard-to-soft state transition, assuming the approaching and receding ejecta were identical. The upper limit of 3.17 kpc corresponds, however, to the minima of both angular velocities and to the bulk Lorentz factor of  $\Gamma \rightarrow \infty$ . The Lorentz factors of the transient ejecta measured in X-ray binaries are

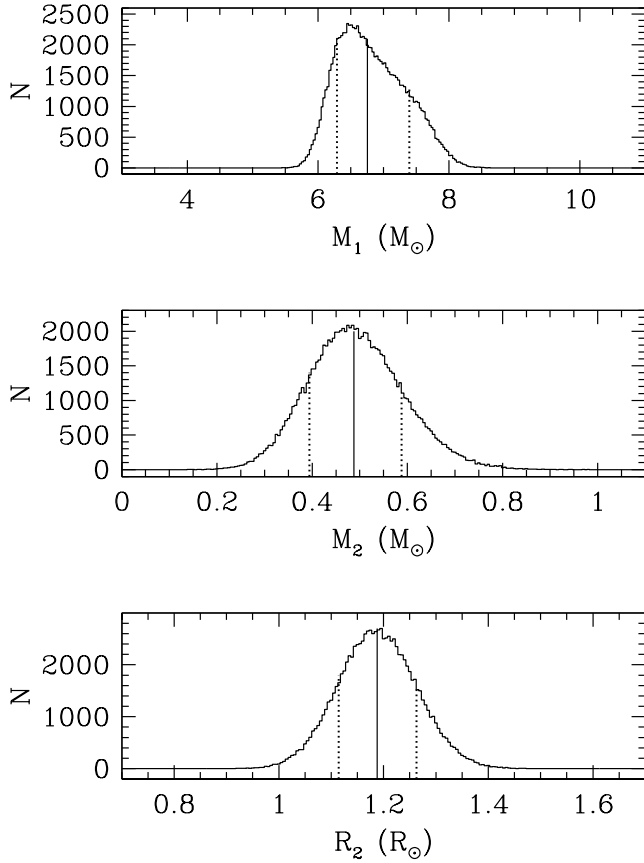


**Figure 1.** The results of Monte Carlo simulations (sampled  $10^5$  times each) of the probability distribution for (top) the mass of the BH, (middle) the donor mass, and (bottom) the donor radius. The vertical solid lines mark the median, and the dashed lines show the 68% confidence, ranges.

generally low, at most a few (Miller-Jones et al. 2006). In the present case,  $D = 3$  and 3.1 kpc correspond to rather large  $\Gamma \geq 3.4$  and 5.1, respectively. Therefore, the measurement by Wood et al. (2021) appears to imply  $D \lesssim 3$  kpc for realistic ejecta Lorentz factors.

The binary orbital period is  $P = 0.68549 \pm 0.00001$  d (Torres et al. 2019) and the inclination of the binary is constrained at  $3\sigma$  to  $i \approx 66.2^\circ - 80.8^\circ$  (Torres et al. 2020). While the latter is consistent with the inclination of the jet,  $i_j \approx 64 \pm 5^\circ$  (Atri et al. 2020; Wood et al. 2021), the jet and binary axes have been estimated to be strongly misaligned (Poutanen et al. 2022), in which case the jet inclination cannot be used to constrain the system masses.

Torres et al. (2020) established the rotational line broadening of the companion of  $v_{\text{rot}} \sin i = 84 \pm 5 \text{ km s}^{-1}$ , which in combination of the radial velocity semi-amplitude ( $K_2 = 417.7 \pm 3.9 \text{ km s}^{-1}$ ) yields (assuming corotation and Roche-lobe filling) the mass ratio of  $q = M_2/M_1 \approx 0.072 \pm 0.012$ , where  $M_1$  and  $M_2$  are the masses of the BH and its companion star. These uncertainties are 1- $\sigma$ . Torres et al. (2020), following Marsh et al. (1994), obtained 2- $\sigma$  limits of  $5.73 < M_1/M_\odot < 8.34$  and  $0.28 < M_2/M_\odot < 0.77$  by combining

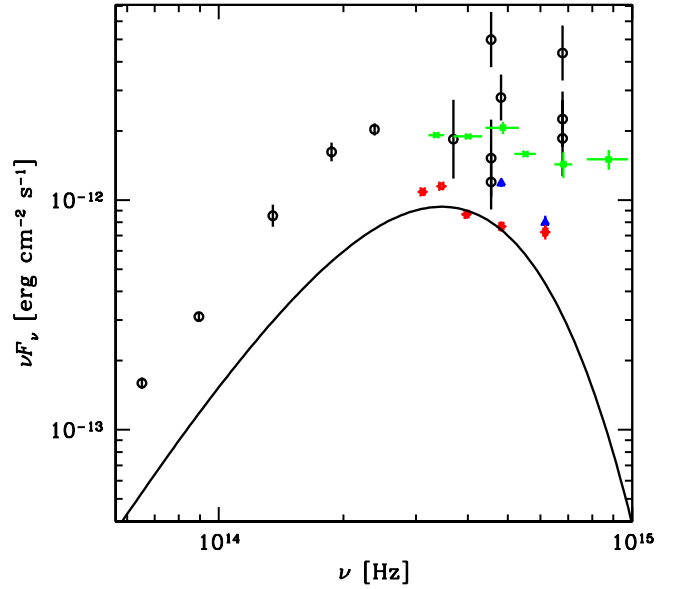


**Figure 2.** The extinction-corrected spectra of the binary during its quiescent states assuming  $E(B-V) = 0.23$ . The red and blue symbols give the minimum fluxes measured by PS1 and ZTF, respectively; see Table 1. The black error bars give the fluxes from the observations listed in Table 2. The green error bars show the average spectrum obtained by Poutanen et al. (2022), see Table 3. The black solid curve show the blackbody with  $R_2 = 1.11 R_\odot$ ,  $D = 3$  kpc and  $T = 4230$  K, whose  $i$ -band flux is at the upper limit of the PS1 measurement, see Equation (3) below. The amplitude of the flux variability due to ellipsoidal variability is  $\lesssim \pm 10\%$  only.

the 1- $\sigma$  uncertainties in the measured orbital parameters with the extreme limits for the range of allowed inclinations. On the other hand, here we have performed Monte Carlo simulations assuming Gaussian distributions of  $v_{\text{rot}} \sin i$  and  $K_2$  (which give  $q$  via eq. 4 of Ziółkowski & Zdziarski 2017),  $P$ , and a flat distribution of  $\cos i$  within the range given above. This gives us probabilistic estimates of  $M_1$  and  $M_2$  and the donor radius,  $R_2 [= P(v_{\text{rot}} \sin i)/(2\pi \sin i)]$ . The results are shown in Figure 1, and they imply  $M_2 = 0.49^{+0.10}_{-0.10} M_\odot$ ,  $R_2 = 1.19^{+0.08}_{-0.08} R_\odot$  and  $M_1 = 6.75^{+0.64}_{-0.46} M_\odot$ , where we give the median and the 68% confidence ranges. Since the radii of main-sequence stars can be roughly approximated by  $R_{\text{MS}}/R_\odot \approx (M/M_\odot)^{0.9}$ , the above range of the donor radius implies that the donor is a moderately evolved star (a subgiant).

The donor average spectrum from observations by the Gran Telescopio Canarias (GTC) during the quiescence after the outburst was found to approximately match those of K3–5 V main-sequence templates (Torres et al. 2020). The effective temperatures of those stars are given by Pecaut & Mamajek (2013) as 4840–4450 K. We have, however, re-analyzed that spectrum and found a strict limit of  $T > 4200$  K based on the lack of molecular bands (TiO and CN) expected at  $T \leq 4200$  K. This limit approximately corresponds to a K6 stellar type, and we use it in our analyses below.

**Table 1.** The minimum observed fluxes for MAXI J1820+070

Source	Band	$\langle\lambda\rangle$ [ $\mu\text{m}$ ]	$F_{\nu,\text{obs}}$ [ $\mu\text{Jy}$ ]	$\langle F_{\nu,\text{obs}}\rangle$ [ $\mu\text{Jy}$ ]	$10^{A_\lambda/2.5}$	Dates
PS1	<i>y</i>	0.963	$265 \pm 10$	$290 \pm 3$	1.33	2011-09-11, 2012-03-30
PS1	<i>z</i>	0.868	$238 \pm 1$	$256 \pm 1$	1.40	2013-04-24
PS1	<i>i</i>	0.755	$141 \pm 6$	$220 \pm 1$	1.55	2013-05-31
PS1	<i>r</i>	0.622	$89.8 \pm 4.5$	$197 \pm 1$	1.77	2013-05-31, 2013-06-19
PS1	<i>g</i>	0.487	$54.9 \pm 3.9$	$117 \pm 1$	2.15	2012-06-11, 2013-06-10
ZTF	<i>r</i>	0.622	$139 \pm 5$		1.77	2021-02-09
ZTF	<i>g</i>	0.487	$60.4 \pm 4.1$		2.15	2020-10-13

NOTE—Here and in Tables 2 and 3,  $F_{\nu,\text{obs}}$  is the observed flux and the intrinsic one is  $F_{\nu,\text{obs}}10^{A_\lambda/2.5}$  for  $E(B-V) = 0.23$  ( $1 \text{ Jy} \equiv 10^{-23} \text{ erg cm}^{-2} \text{ s}^{-1} \text{ Hz}^{-1}$ ). For PS1, the values of  $F_{\nu,\text{obs}}$  are averages from pairs of observations separated by  $\lesssim 0.5$  h with the individual fluxes differing by  $<25\%$ , the uncertainties are the errors of those averages. The average fluxes from the PS1 stacked images,  $\langle F_{\nu,\text{obs}}\rangle$ , are given for comparison. For ZTF, the flux uncertainties correspond to the original magnitude uncertainties.

**Table 2.** Selected infrared and optical observations of MAXI J1820+070 in quiescent states

Source	Band	$\langle\lambda\rangle$ [ $\mu\text{m}$ ]	$F_0$ [Jy]	$m_\lambda$	$F_{\nu,\text{obs}}$ [ $\mu\text{Jy}$ ]	$10^{A_\lambda/2.5}$	Date	Reference
WISE	<i>W2</i>	4.6	3631	$17.95 \pm 0.06$	$239^{+14}_{-13}$	1.02	2010-01-14–2010-07-17	Cutri et al. (2021)
WISE	<i>W1</i>	3.35	3631	$17.59 \pm 0.04$	$334^{+12}_{-11}$	1.04	2010-01-14–2010-07-17	Cutri et al. (2021)
2MASS	<i>K</i>	2.22	655	$15.12 \pm 0.12$	$588^{+69}_{-61}$	1.08	1999-07-23	Cutri et al. (2003)
2MASS	<i>H</i>	1.60	1150	$15.44 \pm 0.10$	$764^{+75}_{-69}$	1.13	1999-07-23	Cutri et al. (2003)
2MASS	<i>J</i>	1.26	1580	$15.87 \pm 0.07$	$711^{+45}_{-42}$	1.20	1999-07-23	Cutri et al. (2003)
GSC2.3.2	<i>I</i>	0.812	2681	$17.24 \pm 0.43$	$341^{+166}_{-111}$	1.46	1989–2000	Lasker et al. (2008)
USNO-B1.0	<i>R</i>	0.658	3247	$16.76 \pm 0.30$	$642^{+204}_{-155}$	1.71	1949–1965	Monet et al. (2003)
GSC2.3.2	<i>R</i>	0.658	3247	$18.05 \pm 0.42$	$196^{+69}_{-63}$	1.71	1987–1999	Lasker et al. (2008)
GTC	<i>r'</i>	0.623	3631	$17.61 \pm 0.25$	$328^{+75}_{-67}$	1.77	2019-06-08–2019-08-07	Torres et al. (2019, 2020)
USNO-B1.0	<i>B</i>	0.442	4067	$17.94 \pm 0.30$	$271^{+86}_{-65}$	2.37	1949–1965	Monet et al. (2003)
GSC2.3.2	<i>B</i>	0.442	4067	$18.87 \pm 0.41$	$115^{+53}_{-36}$	2.37	1987–2000	Lasker et al. (2008)

NOTE—See Straizys (1992) for the values of  $F_0$ . The magnitude for GTC gives the mid point of the observed range, and the uncertainty gives that range.

**Table 3.** The average UV–optical spectrum of MAXI J1820+070 observed on 2020-07-20–23

$\nu$ [ $10^{14}$ Hz]	$16.0 \pm 2.7$	$13.5 \pm 1.5$	$11.7 \pm 1.6$	$8.76 \pm 0.99$	$6.82 \pm 0.34$	$5.51 \pm 0.33$	$4.87 \pm 0.45$	$4.01 \pm 0.32$	$3.36 \pm 0.14$
$F_{\nu,\text{obs}}$ [ $\mu\text{Jy}$ ]	$9.99 \pm 1.17$	$14.0 \pm 2.0$	$31.2 \pm 3.3$	$59.5 \pm 5.9$	$87.9 \pm 11.3$	$148 \pm 4$	$238 \pm 15$	$303 \pm 6$	$415 \pm 10$
$10^{A_\lambda/2.5}$	5.39	7.65	4.28	2.92	2.27	1.84	1.62	1.34	1.12

NOTE—The measurements from  $16.0$  to  $8.76 \times 10^{14}$  Hz are from the *Neil Gehrels Swift* Ultraviolet/Optical Telescope, and those from  $6.82$  to  $3.36 \times 10^{14}$  Hz are from the Liverpool Telescope, La Palma (Poutanen et al. 2022). The first row gives the middle frequencies and the band half-widths.

## 2.2. Photometric properties

We have compiled available ultraviolet to mid-infrared measurements of the binary during its quiescence from literature and public databases. These are listed in Tables 1 to 3, which also provide references to the photometric databases that were explored. In order to constrain the spectral distribution of the donor star, the collected fluxes need to be corrected for interstellar extinction. The total reddening through the Galaxy in the direction of the source has been estimated by Schlafly & Finkbeiner (2011) as  $E(B-V) = 0.197$  and

as  $E(B-V) = 0.23$  by Schlegel et al. (1998). Since the source is located  $\approx 0.5$  kpc above the Galactic disk (see Section 2.3), the extinction toward it is likely to equal the total one in the direction of the target. We can also use the relationship between the extinction in the *V*-band ( $A_V$ ) and the H column density ( $N_H$ ) estimated from fitting X-ray data (Güver & Özel 2009),  $N_H = (2.21 \pm 0.09) \times 10^{21} A_V \text{ cm}^{-2}$ . Here  $A_V$  is given by  $A_V = 3.1E(B-V)$ . The values of  $N_H$  obtained from fitting *XMM-Newton* (Kajava et al. 2019), *NICER* (Bharali et al. 2019) and the X-Ray Telescope

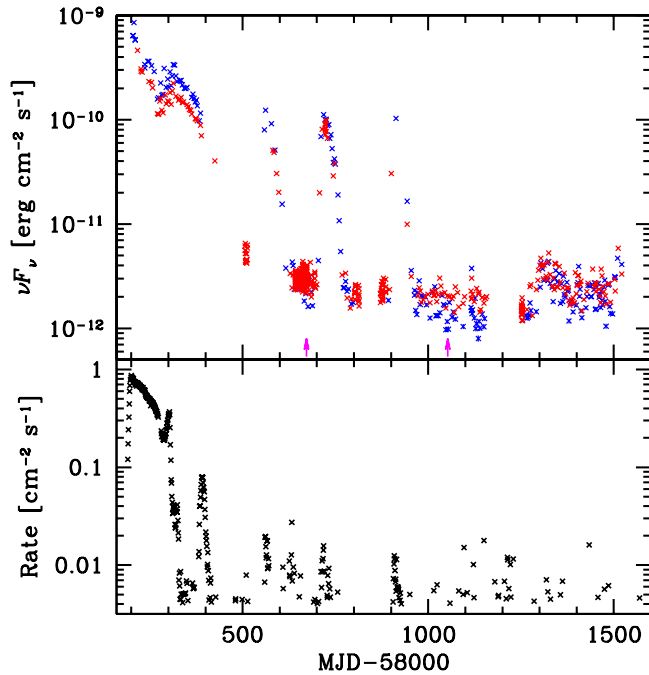


**Figure 3.** Top: the extinction-corrected [assuming  $E(B-V) = 0.23$ ] light curves of the binary from the ZTF. The red and blue symbols correspond to the  $r$  and  $g$  filters, respectively. The two magenta arrows indicate the middle times of the observations of Torres et al. (2019, 2020) and of Poutanen et al. (2022). Bottom: the 15–50 keV daily-averaged count rate from the *Neil Gehrels Swift* BAT. This rate is shown only for  $>0.004 \text{ cm}^{-2} \text{ s}^{-1}$ , at which boundary a typical fractional error is  $\lesssim 0.3$ . We see that major reflares of the source were present until around MJD 58900, then followed by weaker activity in both optical and X-rays.

(Burrows et al. 2000) onboard of *Neil Gehrels Swift* (Wang et al. 2021) data for MAXI J1820+070 are  $1.4^{+0.3}_{-0.3} \times 10^{21}$ ,  $1.6^{+0.3}_{-0.2} \times 10^{21}$ ,  $1.73^{+0.10}_{-0.07} \times 10^{21} \text{ cm}^{-2}$ , respectively. These values correspond (including the uncertainty of the conversion) to the range of  $E(B-V) \approx 0.20\text{--}0.26$ . To calculate the extinction at other wavelengths,  $A_\lambda$ , we used  $A_V$  and the fitting formulae of Cardelli et al. (1989). Then, the observed magnitudes,  $m_\lambda$ , can be transformed into the observed,  $F_{\nu,\text{obs}}$ , and unabsorbed,  $F_\nu$ , fluxes, as

$$F_{\nu,\text{obs}} = F_0 10^{-m_\lambda/2.5}, \quad (1)$$

$$F_\nu = F_{\nu,\text{obs}} 10^{A_\lambda/2.5}, \quad (2)$$

where  $F_0$  is the flux corresponding to a zero magnitude.

We first consider spectral data from Pan-STARRS1<sup>1</sup> Data Release 2 (PS1 DR2), which give measurements in the  $y$ ,  $z$ ,  $i$ ,  $r$  and  $g$  bands for years previous to the outburst. We have searched for the overall minimum fluxes in each photometric band, using the `psfFlux` and `psfFluxErr` values in the Detection Table provided in PS1 DR2. Those fluxes were

obtained using an automated pipeline; thus single detections at the faint end may be not real, but arise from a systematic noise (Chambers et al. 2016), and be indistinguishable from real detections. In order to avoid them, we have applied a stringent selection criterion. Namely, we used *only* double detections from subsequent exposures separated by  $\lesssim 0.5$  h and with the fluxes differing by  $< 25\%$ . The results are given in Table 1 and plotted in red in Figure 2 after correcting for the extinction assuming  $E(B-V) = 0.23$ . For comparison, Table 1 also gives the average fluxes from the DR2 stacked images, which are significantly higher than the minimum fluxes in the  $i$ ,  $r$  and  $g$  bands.

Next, we have obtained the  $r$  and  $g$  light curves observed by the Zwicky Transient Facility<sup>2</sup> (ZTF; Bellm et al. 2019), covering the discovery outburst and subsequent decay up to 2021 August. They are shown in Figure 3. We see that several mini-outbursts or reflares occurred after the end of the main outburst event, with the last major reflare in 2020 April. For comparison, we also show the hard X-ray light curve<sup>3</sup> from the Burst Alert Facility (Barthelmy et al. 2005; BAT) onboard of *Neil Gehrels Swift*. We see that the optical reflares have been accompanied by X-ray activity. From the ZTF light curves, we have obtained the weakest fluxes measured in each filter, which are given in Table 1 and are plotted in blue symbols in Figure 2.

Then, we have compiled some other available optical and infrared measurements of MAXI J1820+070 during quiescence. We list them in Table 2 and plot in Figure 2 with black error bars. Table 2 also gives the values of  $F_0$ . Most of the fluxes are higher than the minima from PS1. In particular, we analyzed the observations made during the states near quiescence in the  $r$  band (of the SDSS photometric system) reported in Torres et al. (2019, 2020). After calibrating the photometry of MAXI J1820+070 against the PSF mean magnitude of a non-variable star in the field, the range of those magnitudes is  $r' \approx 17.87 \pm 0.02\text{--}17.35 \pm 0.02$ , and its midpoint is  $r' \approx 17.6$ . Finally, we plot the average optical and UV fluxes obtained by Poutanen et al. (2022), see Table 3. The arrows in Figure 3 indicate the middle times of the observations of Torres et al. (2019, 2020) and of Poutanen et al. (2022).

The PS1 DR2 minimum fluxes shown in Figure 2 constrain the stellar contribution, which we approximate as a blackbody,  $F_\nu^* = \pi B_\nu(T)(R_2/D)^2$ , where  $B_\nu(T)$  is the blackbody intensity and  $T$  is the effective temperature. The most restrictive measurement is that in the  $i$  band, for which we take its upper limit (Table 1) and assume  $E(B-V) = 0.23$ . We have found that the blackbody relationship for this monochromatic flux can be locally approximated as a power law of  $T \propto (D/R_2)^{0.45}$ . The constraint, together with the temperature limit from our analysis of the average spectrum

<sup>2</sup> [https://irsa.ipac.caltech.edu/docs/program\\_interface/ztf\\_lightcurve\\_api.html](https://irsa.ipac.caltech.edu/docs/program_interface/ztf_lightcurve_api.html)

<sup>3</sup> <https://swift.gsfc.nasa.gov/results/transients/weak/MAXIJ1820p070/>

<sup>1</sup> <https://catalogs.mast.stsci.edu/panstarrs/>

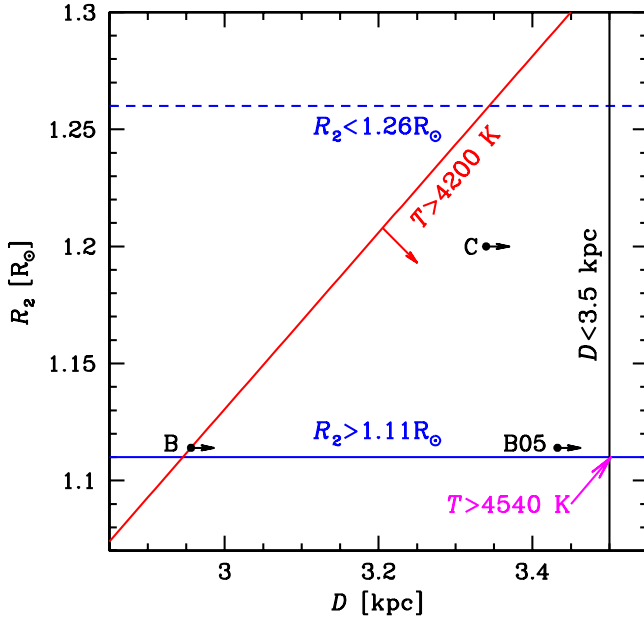


**Figure 4.** The region in the  $D$ – $R_2$  space allowed by the constraints on  $R_2$  from the binary parameters, on  $D$  from the *Gaia* parallax, and on  $T$  from the blackbody [for  $E(B-V) = 0.23$ ] and spectral limits, see Equations (3–4). The horizontal blue solid and dashed lines correspond to the lower and upper limit on  $R_2$  (Section 2.1), respectively; the vertical black solid line gives the limit of  $D \leq 3.5$  kpc, and the diagonal red solid line corresponds to the limiting  $D/R_2$  from the PS1  $i$ -band flux and  $T > 4200$  K at  $A = 1$ . If an accretion disk still contributes to that emission,  $A > 1$ , and the red line moves in the direction of the red arrow becoming steeper. The allowed region is within the lower triangle delineated by the three solid lines. The limit on  $T$  increases diagonally perpendicular to the red line from 4200 K on it to 4540 K at the lower right corner of the allowed space. Three evolutionary models of Section 3, B, B05 and C, satisfy these constraints, and are shown by the black solid circles with arrows (moving horizontally for  $A > 1$ ).

of Torres et al. (2019, 2020), can be written as

$$\frac{D/2.95 \text{ kpc}}{R_2/1.11R_\odot} \gtrsim A \left( \frac{T}{4200 \text{ K}} \right)^{2.22}, \quad (3)$$

$$T > 4200 \text{ K}, \quad (4)$$

where Equation (3) is scaled to the lower limit on the stellar radius, see Section 2.1. Here the constant  $A$  accounts for the accretion disk being expected to be present at some level during the entire quiescence (see, e.g., the models of Dubus et al. 2001), in which case  $A > 1$ . On the other hand, the flux measurements may be affected by ellipsoidal variability, whose full amplitude we estimate as  $< 0.2$  mag, i.e., less than  $\pm 10\%$  with respect the average flux. This estimate is based on the ellipsoidal variability of the BH LMXB A0620–00, which has the mass ratio  $q = 0.067 \pm 0.01$  (Marsh et al. 1994) and  $66^\circ.5 < i < 73^\circ.5$  (Haswell et al. 1993), consistent within the uncertainties with those of MAXI J1820+070. The full amplitude of the ellipsoidal variability of A0620–00

was measured by Marsh et al. (1994) as 0.13 mag. They also performed detailed simulations of this effect for a range of the inclinations, and their table 4 gives the theoretical range of 0.15–0.18 mag at  $i = 70^\circ$ . Given the relative weakness of this effect, we neglect it. We also set  $A = 1$ . The fiducial distance of 3 kpc and the minimum  $R_2$  correspond to  $T \leq 4230$  K. We plot a blackbody spectrum at  $T = 4230$  K in the solid black curve in Figure 2. This spectrum gives a  $\approx 26\%$  contribution [at  $E(B-V) = 0.23$ ] to the average flux in the  $r$  band of Torres et al. (2019, 2020). This is moderately higher than the stellar contribution of 16–21% estimated by them.

Equations (3–4) for  $R_2 \gtrsim 1.11R_\odot$  imply a  $D \gtrsim 2.95$  kpc, in agreement with all the constraints on  $D$  listed in Section 2.1. On the other hand, these equations do not constrain  $D$  from above. We take here  $D \lesssim 3.5$  kpc from the *Gaia* parallax as a tentative conservative upper limit. While the limit of Wood et al. (2021) is stringent at face value, it relies on the two ejecta being exactly symmetric, which may not be the case, and 3.5 kpc is within the  $2\sigma$  uncertainty of the radio parallax, see Section 2.1. We plot the resulting joint constraints on  $D$  and  $R_2$  in Figure 4. At  $D = 3.5$  kpc and  $R_2 = 1.11R_\odot$ , we have the maximum  $T \approx 4540$  K, corresponding to a K5 stellar type. This satisfies the original constraint of Torres et al. (2020). We note that the above constraints favor low donor radii if  $D \lesssim 3$  kpc. At  $D \leq 3$  kpc and  $T = 4200$  K,  $R_2 \leq 1.13R_\odot$ . Note that the above constraints can still be relaxed if there are some systematic error on the minimum PS1 fluxes, present in spite of our strict selection procedure.

### 2.3. Metallicity

MAXI J1820+070 appears to be a relatively old system and thus may have come from an environment with a sub-solar metallicity. Its position in the Cartesian coordinates  $(X, Y, Z)$  centered on the Sun and the velocities calculated from the coordinated proper motion,  $\text{pmRA} = -3.093 \pm 0.091$  mas/yr and  $\text{pmDec} = -6.283 \pm 0.094$  mas/yr (*Gaia* EDR3, Gaia Collaboration et al. 2021), the systemic velocity of  $\gamma = -22$  km/s (Torres et al. 2019) and the adopted distance of  $D = 3$  kpc, are

$$X = 2393 \text{ pc}, Y = 1730 \text{ pc}, Z = 529 \text{ pc}, \quad (5)$$

$$U = 40.85 \text{ km/s}, V = -93.40 \text{ km/s}, W = -4.19 \text{ km/s},$$

where  $U, V, W$  are velocities along the same axes, with  $X, U$  positive towards the Galactic center,  $Y, V$  positive in the direction of the Sun motion around the Galaxy, and  $Z, W$  positive out of the plane of the Galaxy. MAXI J1820+070 is thus located in the thick Galactic disk as indicated by its distance from the Galactic plane,  $Z = 529$  pc, and a high peculiar velocity,  $V_{\text{pec}} = 94$  km/s, moving almost parallel to the Galactic plane. The Galactic  $U, V, W$  velocities also locate it among the extended thick-disk population objects in Toomre diagram (e.g. fig. 1 in Feltzing et al. 2003). The Galactocentric distance of MAXI J1820+070 is 5.9 kpc, which locates it in the inner Galactic disk, where the average value of the metallicity is  $\langle [\text{Fe}/\text{H}] \rangle = -0.55 \pm 0.17$  (e.g.

Bensby et al. 2011). The subsolar metallicity of the donor is further supported by relatively strong Ca I and Ti I absorption lines compared to Fe I lines in the spectrum presented in fig. 3 of (Torres et al. 2019), similar to other thick disk objects (e.g. Feltzing et al. 2003).

We also note that high peculiar velocities of BH LMXBs are often attributed to a BH natal kick velocity, see, e.g. Atri et al. (2019). That study included MAXI J1820+070 and three other systems with no known (at that time) systemic velocities and accurate distances, using instead a hypothetical kick velocity distribution modelled by Monte Carlo simulations. Based on them, they tentatively preferred the natal kick origin of the peculiar velocity in MAXI J1820+070. Still, they also note that most LMXBs are relatively old systems, and thus may have come from low metallicity environments like globular clusters.

On the other hand, metallicities higher than solar were found in a number of donor stars in LMXBs (see review in Casares et al. 2017). Still, this does not appear to be universal. One example is the binary V934 Her/4U 1700+24 consisting of a red giant accreting on a neutron star. Detailed photospheric abundance analysis for this system resulted in a slightly subsolar metallicity,  $[\text{Fe}/\text{H}] \approx -0.5$  and  $[\alpha/\text{Fe}] = +0.27$  (where  $\alpha$  represents the average of the Mg, Si, and Ca elements), and the  $[\alpha/\text{Fe}]$  versus  $[\text{Fe}/\text{H}]$  relation close to the mean one without any notable peculiarity to this object (Hinkle et al. 2019). Similar  $\alpha$ -element and Fe abundances were found in many symbiotic giants with white dwarf companions (Gafan et al. 2016, 2017).

#### 2.4. Average mass transfer rate

The bolometric flux of the source varied within only a factor of 2–3 during most of the 2018 discovery outburst, i.e.,  $\approx 200$  d, see, e.g., Shidatsu et al. (2019), Fabian et al. (2020), namely within  $\approx (0.5\text{--}1.5) \times 10^{-7} \text{ erg cm}^{-2} \text{ s}^{-1}$ . In order to estimate the total fluence of that outburst, we adopt the flux of  $1.0 \times 10^{-7} \text{ erg cm}^{-2} \text{ s}^{-1}$  during 200 d. Assuming  $D = 3 \text{ kpc}$  and the accretion efficiency of  $\epsilon = 0.1$ , we obtain the accreted mass of  $M_{\text{accr}} \approx 2 \times 10^{25} \text{ g}$ . However, given the uncertainties on the fluence, distance and accretion efficiency, the uncertainty of this mass is probably by a factor of two.

After the 2018 discovery outburst, two historical outbursts in 1898 and 1934 were discovered by examining publicly available photographic plates (Kojiguchi et al. 2019). Based on these data, the typical interval between outbursts of this source was estimated by those authors as 40 yr. This implies that the outburst within 1970–1980 was missed by observers of the period. However, intervals between outbursts of BH LMXBs are often unequal, and it is also possible that there was no outburst since 1934, giving the interval from the previous outburst of 84 yr. If we assume that the mass accreted onto the BH in 2018 equals to that transferred from the donor during the interval since the previous outburst (which theoretical assumption is clearly uncertain), the average mass transfer rate is  $-\dot{M}_2 \approx 1.2 \times 10^{-10} \text{ M}_{\odot}/\text{yr}$ , with an uncertainty, which we estimate to be by a factor of two. Alternatively, the

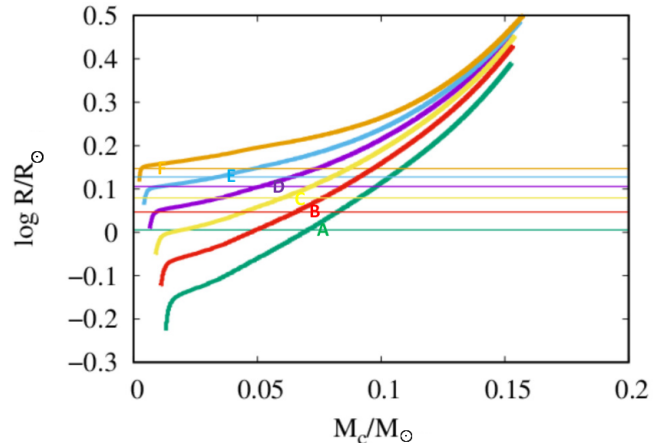


**Figure 5.** The radii of partially stripped, moderately evolved stars with solar metallicity vs. the mass of the He core for total donor masses of  $M_2 = 0.3, 0.4, 0.5, 0.6, 0.7$  and  $0.8 \text{ M}_{\odot}$ . They are shown (from bottom to top) by the green, red, yellow, violet, blue and orange thick solid curves, respectively. The evolution proceeds from left to right at the constant  $M_2$ . The horizontal dashed lines with the corresponding colors (from bottom to top) show the radii of the Roche lobe around the donor for the above values of  $M_2$  (almost independent of  $M_1$ ). The crossings of the corresponding evolutionary tracks and horizontal lines determine the positions of the models.

estimate of  $-\dot{M}_2$  would increase to  $\approx 2.6 \times 10^{-10} \text{ M}_{\odot}/\text{yr}$  if the actual interval between outbursts was 40 yr.

### 3. THE EVOLUTIONARY STATUS

We use the Warsaw stellar evolution code of Paczyński (1969, 1970) described in Pamyatnykh et al. (1998) and Ziółkowski (2005). Our version of the code is calibrated to yield the H mass fraction of  $X = 0.74$ , the metallicity of  $Z = 0.014$  (we use here the symbols  $X$  and  $Z$  in a different meaning than in Section 2.3), and the mixing length parameter of 1.55 for the Sun at the solar age. The method of the evolutionary calculations in this work follow those used in Ziółkowski & Zdziarski (2017, 2018) and Zdziarski et al. (2019). We refer the reader to Zdziarski et al. (2019) for details of the method.

We have first followed the evolution in the core mass–stellar radius plane of partially stripped stars for total masses of  $M_2 = 0.3, 0.4, 0.5, 0.6, 0.7$  and  $0.8 \text{ M}_{\odot}$  and at the solar metallicity. The results are shown in Figure 5 and Table 4, where these models are denoted by letters A, B, C, D, E and F, respectively. In Figure 5, the evolution proceeds from left to right at the constant  $M_2$ . The evolutionary engine lies in the hydrogen burning shell, which adds newly synthesized helium to the core, increasing its mass. The horizontal thin lines with the corresponding colors (from bottom to top) show the radii of the Roche lobe around the donor for the above values of  $M_2$ , and  $M_1 = 7 \text{ M}_{\odot}$ . The crossings of the corresponding evolutionary tracks and horizontal lines determine the positions of our donor models. The relatively small core masses of those models confirm that the donor is

**Table 4.** The results of the evolutionary calculations for the donor

Model	$\frac{M_2}{M_\odot}$	$\frac{R_2}{R_\odot}$	$\frac{L_2}{L_\odot}$	$T$ [K]	$\frac{M_c}{M_\odot}$	$-\dot{M}_{2,10}$
A	0.3	1.012	0.278	4169	0.070	0.43
A2	0.3	1.012	0.219	3924	0.290	0.155
<b>B05</b>	0.4	1.114	0.452	4492	0.050	1.0
<b>B</b>	0.4	1.114	0.347	4200	0.065	0.68
B2	0.4	1.114	0.273	3948	0.084	0.27
C05	0.5	1.200	0.587	4621	0.042	1.3
<b>C</b>	0.5	1.200	0.437	4289	0.060	0.91
D	0.6	1.275	0.560	4430	0.051	1.1
D2	0.6	1.275	0.414	4102	0.130	0.49
E	0.7	1.343	0.749	4643	0.034	1.25
F	0.8	1.404	1.019	4903	0.003	1.55

NOTE— $M_c$  is the mass of the He core, and  $-\dot{M}_{2,10}$  is the stellar mass loss rate in units of  $10^{-10}M_\odot \text{ yr}^{-1}$ . The BH mass of  $M_1 = 7M_\odot$  was assumed. The models denoted by a single letter have the solar metallicity  $Z = 0.014$ , while models A2, B2 and D2 have  $Z = 0.028$ , and B05 and C05 have  $Z = 0.007$ . Model B is at the minimum temperature allowed by the GTC spectrum and corresponds to  $D \gtrsim 2.9$  pc. Model B05 has the temperature approximately best-fitting the spectrum, but it requires  $D \gtrsim 3.4$  kpc. Model C has an intermediate temperature and  $D \gtrsim 3.3$  kpc. These models are marked in Figure 4.

in an early subgiant phase, with the radius only a factor of about two larger than a main-sequence star of the same mass (as noticed in Section 2.1). Given that the donor metallicity is relatively uncertain (Section 2.3), we also calculated some models for a metallicity of half solar,  $Z = 0.007$  (B05 and C05), and twice solar,  $Z = 0.028$ , (A2, B2 and D2), whose results are also given in Table 4. The seen anticorrelation of the metallicity and temperature in our evolutionary models is a well-known effect, resulting from an increase of the opacities with the metallicity, present also in main sequence stars.

The assumed BH mass,  $M_1$ , influences only one model parameter, namely the rate of the mass transfer,  $-\dot{M}_2$ . However, this effect is rather weak. For models A and F, changing  $M_1$  to  $3.17M_\odot$  and  $11.1M_\odot$ , respectively (to keep the mass ratio equal 0.072), would change  $-\dot{M}_2$  from 4.3 to  $4.4 \times 10^{-11}M_\odot/\text{yr}$ , and from 1.55 to  $1.50 \times 10^{-10}M_\odot/\text{yr}$ , respectively.

We compare now the models of Table 4 with the Monte Carlo constraints obtained in Section 2.1 and other constraints obtained in Sections 2.2, 2.3 and 2.4. As shown based on the fluxes measured before the outburst (Section 2.2), an approximate maximal stellar blackbody contribution at  $D = 3$  kpc has  $T = 4200$  K and  $R_2 = 1.13R_\odot$ . This closely corresponds to our model B, which support an approximate solar metallicity of the donor. If we still impose the spectral type to be within K5–K3 (which requires  $D \sim 3.5$  kpc), the temperature has to be larger, which approximately cor-

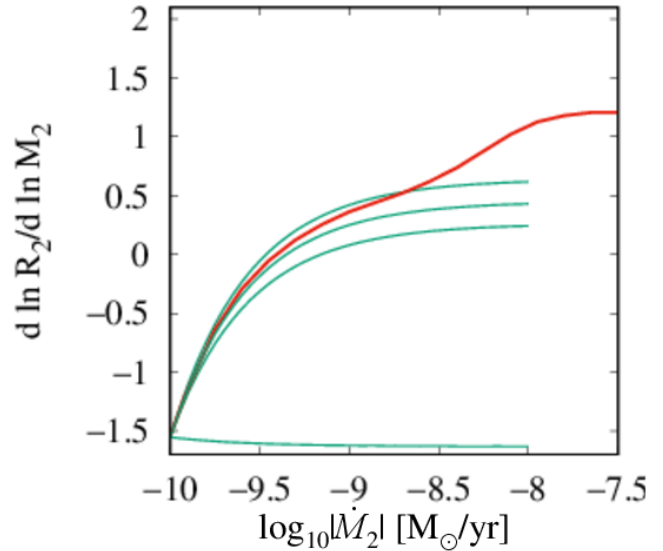


**Figure 6.** The rates of the evolutionary change of the donor radius (red curve) and that of its Roche lobe (green curves) as functions of the donor mass loss rate,  $-\dot{M}_2$ . The conservative solution corresponds to model B05, with the averaged accretion rate on the BH of  $\langle \dot{M}_1 \rangle = 1.0 \times 10^{-10}M_\odot \text{ yr}^{-1}$ . The results of our evolutionary model include now the effect of mass outflow from the outer layers of the star. The green curves show  $d \ln R_{2,L}/d \ln M_2$  for  $\alpha = 0, 1, 1.1, \text{ and } 1.2$ , from bottom to top. The values of  $\beta$  along those curves are given by  $\langle \dot{M}_1 \rangle / |\dot{M}_2|$ , i.e.,  $\beta = 1$  at the beginnings of the green curves. The intersection of the red curve and the top green one gives a possible self-consistent and non-conservative model of MAXI J1820+070, see Section 3.

responds to our model B05 with  $T = 4492$  K. This model has half-solar metallicity, which agrees with the finding of Section 2.3 that MAXI J1820+070 is likely to belong to extended Galactic thick disk population. On the other hand, it is in tension with the X-ray spectral fitting of Zdziarski et al. (2021), which favor the metallicity to be at least solar. Our model C, with  $M_2 = 0.5M_\odot$  and  $R_2 = 1.2R_\odot$ , also satisfies our constraints, yielding  $T = 4289$  K and  $D \gtrsim 3.3$  kpc. These three models are shown in the  $R_2$ – $D$  parameter space in Figure 4. We see that the constraints shown on Figure 4 allow the metallicity to be only slightly above solar. On the other hand, our models with metallicity twice solar, A2, B2 and D2, have the temperatures of 3924 K–4102 K, which are below our strict lower limit of 4200 K.

The calculated mass-loss rate for model B05 is  $-\dot{M}_2 \approx 1.0 \times 10^{-10}M_\odot/\text{yr}$ , which agrees well with that estimated in Section 2.4 of  $1.2 \times 10^{-10}M_\odot/\text{yr}$  with an uncertainty by a factor of two. For model B,  $-\dot{M}_2$  is only slightly lower.

The above agreement implies that the mass loss rate approximately equals the accretion rate averaged over the interval since the previous outburst,  $\langle \dot{M}_1 \rangle$ , i.e., the mass transfer is conservative. However, this assumption is uncertain, with outflows and not full exhaustion of the disk during outburst being possible. Indeed, mass loss from a disk wind in MAXI

J1820+070 was found by Muñoz-Darias et al. (2019). This motivates us to consider also models with non-conservative mass transfer. We note that taking this effect into account does not change the model parameters of the donor. It only increases the model values of  $-\dot{M}_2$ . We consider here non-conservative mass transfer for model B05, following the approach of Ziółkowski & Zdziarski (2018). Such transfer is described by two parameters,  $\alpha$  and  $\beta$ . As in Ziółkowski & Zdziarski (2018), we define  $\alpha$  as the specific angular momentum of the mass leaving the system in units of the specific angular momentum of the donor measured from the center of mass (Verbunt 1993), with  $\alpha \lesssim 1$  (as discussed, e.g., in Ziółkowski & Zdziarski 2018). The parameter  $\beta$  is defined as the fraction of the mass lost by the donor that is accreted onto the accretor (Rappaport et al. 1982), i.e.,  $-\dot{M}_2 = \langle \dot{M}_1 \rangle / \beta$ .

We assume  $\langle \dot{M}_1 \rangle = 1.0 \times 10^{-10} M_\odot \text{ yr}^{-1}$ . The results are shown in Fig. 6. We compare here the rates of the Roche-lobe change for  $\alpha = 0, 1, 1.1$  and  $1.2$  with the rate implied by our evolutionary model as a function of  $\beta = \langle \dot{M}_1 \rangle / |\dot{M}_2|$ . Apart from the conservative solution ( $\beta = 1$ ), a non-conservative solution is possible for  $\beta \approx 0.05$  and  $\alpha = 1.2$ . A caveat for it is its relatively large  $\alpha$ , requiring the outflow to occur far from the BH, around the disk tidal radius (see fig. 1 of Ziółkowski & Zdziarski 2018). Thus, the simplest and most likely solution remains the conservative case.

#### 4. SUMMARY

We have used the  $1\text{-}\sigma$  deviations for the binary parameters of MAXI J1820+070 and a uniform distribution in  $\cos i$  for the range of inclinations given in Torres et al. (2020) to calculate the donor star mass and radius. We obtain 68% confidence values of  $M_2 = 0.49^{+0.10}_{-0.10} M_\odot$  and  $R_2 = 1.19^{+0.08}_{-0.08} R_\odot$  (as well as  $M_1 = 6.75^{+0.64}_{-0.46} M_\odot$  for the BH mass).

We have compiled available optical and infrared measurements of MAXI J1820+070 in quiescence, which constrain the spectrum of the donor. The strongest constraint is given by the minimum fluxes from PS1 DR2 in the  $i$  and  $r$  bands, which gives the maximum allowed blackbody temperature of  $T < 4230$  K at the lower limit on the donor radius allowed by the binary parameters ( $R_2 = 1.11 R_\odot$ ),  $D \approx 3$  kpc and  $E(B-V) = 0.23$ . This  $T$  is at our lower limit of the temperature compatible with the average GTC spectrum of  $T > 4200$  K, and it is less than those implied by the original classification of the stellar type of the donor within the range of K3–5 (Tor-

res et al. 2020). Requiring the latter can be reconciled with our constraints if  $D \sim 3.5$  kpc, yielding  $T \lesssim 4540$  K, of a K5 stellar type. The distance of  $D = 3.5$  kpc is allowed by the *Gaia* parallax, but it is larger than those obtained from the radio parallax and the moving ejecta method.

We then considered the source location in the Galaxy and peculiar velocity, which indicate MAXI J1820+070 belongs to the extended thick-disk population. That population is characterized by the metallicity less than solar. We also estimated the fluence during the 2018 outburst. Using the time elapsed since the previous detected outburst of the system, we evaluate the average mass accretion rate (equal to the average transfer rate for conservative accretion) of  $-\dot{M}_2 \sim 10^{-10} M_\odot/\text{yr}$ .

We finally considered a range of stellar evolutionary models that may correspond to MAXI J1820+070. Our model B (see Table 4) approximates the above constraints at the limiting  $T = 4200$  K, the donor mass of  $M_2 = 0.4 M_\odot$  and the solar metallicity (which approximately agrees with the X-ray spectral fitting results of Zdziarski et al. 2021) and requires  $D \geq 3$  kpc. An alternative at  $D \gtrsim 3.3$  kpc is our model C with  $T \approx 4300$  K. Another possibility at  $D \gtrsim 3.3$  kpc is our model B05, with  $T \approx 4500$  K and the metallicity half solar, which, in turn, agrees with the location of the source in the Galaxy. Thus, we cannot unambiguously constrain the donor metallicity. Still, we find models with the metallicity twice solar to be ruled out.

We also considered evolutionary models with non-conservative accretion. However, we have found they require an unrealistically large specific angular momentum of the mass leaving the system.

#### ACKNOWLEDGMENTS

We thank Juri Poutanen for providing us with their average optical-ultraviolet spectrum of MAXI J1820+070, and the referee for valuable suggestions. We acknowledge support from the Polish National Science Centre under the grants 2015/18/A/ST9/00746, 2019/35/B/ST9/03944 and 2017/27/B/ST9/01940. AAZ acknowledges support from the International Space Science Institute (Bern). MAPT and JCV have been supported by the Spanish MINECO under grant AYA2017-83216-P and PID2020-120323GB-I00. MAPT acknowledge support via a Ramón y Cajal Fellowship RYC-2015-17854.

#### REFERENCES

- Atri, P., Miller-Jones, J. C. A., Bahramian, A., et al. 2019, MNRAS, 489, 3116, doi: [10.1093/mnras/stz2335](https://doi.org/10.1093/mnras/stz2335)
- . 2020, MNRAS, 493, L81, doi: [10.1093/mnras/slaa010](https://doi.org/10.1093/mnras/slaa010)
- Bailer-Jones, C. A. L., Rybizki, J., Foesneau, M., Demleitner, M., & Andrae, R. 2021, AJ, 161, 147, doi: [10.3847/1538-3881/abd806](https://doi.org/10.3847/1538-3881/abd806)
- Barthelmy, S. D., Barbier, L. M., Cummings, J. R., et al. 2005, SSRv, 120, 143, doi: [10.1007/s11214-005-5096-3](https://doi.org/10.1007/s11214-005-5096-3)
- Bellm, E. C., Kulkarni, S. R., Graham, M. J., et al. 2019, PASP, 131, 018002, doi: [10.1088/1538-3873/aaecbe](https://doi.org/10.1088/1538-3873/aaecbe)
- Bensby, T., Alves-Brito, A., Oey, M. S., Yong, D., & Meléndez, J. 2011, ApJL, 735, L46, doi: [10.1088/2041-8205/735/2/L46](https://doi.org/10.1088/2041-8205/735/2/L46)
- Bharali, P., Chauhan, J., & Boruah, K. 2019, MNRAS, 487, 5946, doi: [10.1093/mnras/stz1686](https://doi.org/10.1093/mnras/stz1686)
- Buisson, D. J. K., Fabian, A. C., Barret, D., et al. 2019, MNRAS, 490, 1350, doi: [10.1093/mnras/stz2681](https://doi.org/10.1093/mnras/stz2681)



- Burrows, D. N., Hill, J. E., Nousek, J. A., et al. 2000, *Proc. SPIE*, 4140, 414064, doi: [10.1117/12.409158](https://doi.org/10.1117/12.409158)
- Cardelli, J. A., Clayton, G. C., & Mathis, J. S. 1989, *ApJ*, 345, 245, doi: [10.1086/167900](https://doi.org/10.1086/167900)
- Casares, J., Jonker, P. G., & Israelian, G. 2017, in *X-Ray Binaries*, ed. A. W. Alsabti & P. Murdin (Springer), 1499–1526, doi: [10.1007/978-3-319-21846-5\\_111](https://doi.org/10.1007/978-3-319-21846-5_111)
- Chambers, K. C., Magnier, E. A., Metcalfe, N., et al. 2016, arXiv e-prints, arXiv:1612.05560. <https://arxiv.org/abs/1612.05560>
- Cutri, R. M., Skrutskie, M. F., van Dyk, S., et al. 2003, *VizieR Online Data Catalog*, II/246
- Cutri, R. M., Wright, E. L., Conrow, T., et al. 2021, *VizieR Online Data Catalog*, II/328
- Dubus, G., Hameury, J.-M., & Lasota, J.-P. 2001, *A&A*, 373, 251, doi: [10.1051/0004-6361:20010632](https://doi.org/10.1051/0004-6361:20010632)
- Fabian, A. C., Buisson, D. J., Kosec, P., et al. 2020, *MNRAS*, 493, 5389, doi: [10.1093/mnras/staa564](https://doi.org/10.1093/mnras/staa564)
- Feltzing, S., Bensby, T., & Lundström, I. 2003, *A&A*, 397, L1, doi: [10.1051/0004-6361:20021661](https://doi.org/10.1051/0004-6361:20021661)
- Gaia Collaboration, Brown, A. G. A., Vallenari, A., et al. 2021, *A&A*, 649, A1, doi: [10.1051/0004-6361/202039657](https://doi.org/10.1051/0004-6361/202039657)
- Gałań, C., Mikołajewska, J., Hinkle, K. H., & Joyce, R. R. 2016, *MNRAS*, 455, 1282, doi: [10.1093/mnras/stv2365](https://doi.org/10.1093/mnras/stv2365)
- . 2017, *MNRAS*, 466, 2194, doi: [10.1093/mnras/stw3266](https://doi.org/10.1093/mnras/stw3266)
- García, J. A., Kallman, T. R., Bautista, M., et al. 2018, in *Astronomical Society of the Pacific Conference Series*, Vol. 515, *Workshop on Astrophysical Opacities*, 282. <https://arxiv.org/abs/1805.00581>
- Güver, T., & Özel, F. 2009, *MNRAS*, 400, 2050, doi: [10.1111/j.1365-2966.2009.15598.x](https://doi.org/10.1111/j.1365-2966.2009.15598.x)
- Haswell, C. A., Robinson, E. L., Horne, K., Stiening, R. F., & Abbott, T. M. C. 1993, *ApJ*, 411, 802, doi: [10.1086/172884](https://doi.org/10.1086/172884)
- Hinkle, K. H., Fekel, F. C., Joyce, R. R., et al. 2019, *ApJ*, 872, 43, doi: [10.3847/1538-4357/aafba5](https://doi.org/10.3847/1538-4357/aafba5)
- Kajava, J. J. E., Motta, S. E., Sanna, A., et al. 2019, *MNRAS*, 488, L18, doi: [10.1093/mnras/slz089](https://doi.org/10.1093/mnras/slz089)
- Kawamuro, T., Negoro, H., Yoneyama, T., et al. 2018, *Astron. Telegram*, 11399, 1
- Kojiguchi, N., Kato, T., Isogai, K., & Nogami, D. 2019, *The Astronomer's Telegram*, 13066, 1
- Lasker, B. M., Lattanzi, M. G., McLean, B. J., et al. 2008, *AJ*, 136, 735, doi: [10.1088/0004-6256/136/2/735](https://doi.org/10.1088/0004-6256/136/2/735)
- Marsh, T. R., Robinson, E. L., & Wood, J. H. 1994, *MNRAS*, 266, 137, doi: [10.1093/mnras/266.1.137](https://doi.org/10.1093/mnras/266.1.137)
- Miller-Jones, J. C. A., Fender, R. P., & Nakar, E. 2006, *MNRAS*, 367, 1432, doi: [10.1111/j.1365-2966.2006.10092.x](https://doi.org/10.1111/j.1365-2966.2006.10092.x)
- Mirabel, I. F., & Rodríguez, L. F. 1994, *Nature*, 371, 46, doi: [10.1038/371046a0](https://doi.org/10.1038/371046a0)
- Monet, D. G., Levine, S. E., Canzian, B., et al. 2003, *AJ*, 125, 984, doi: [10.1086/345888](https://doi.org/10.1086/345888)
- Muñoz-Darias, T., Jiménez-Ibarra, F., Panizo-Espinar, G., et al. 2019, *ApJL*, 879, L4, doi: [10.3847/2041-8213/ab2768](https://doi.org/10.3847/2041-8213/ab2768)
- Paczyński, B. 1969, *AcA*, 19, 1
- . 1970, *AcA*, 20, 47
- Pamyatnykh, A. A., Dziembowski, W. A., Handler, G., & Pikall, H. 1998, *A&A*, 333, 141. <https://arxiv.org/abs/astro-ph/9801264>
- Pecaut, M. J., & Mamajek, E. E. 2013, *ApJS*, 208, 9, doi: [10.1088/0067-0049/208/1/9](https://doi.org/10.1088/0067-0049/208/1/9)
- Poutanen, J., Veledina, A., Berdyugin, A. V., et al. 2022, *Science*, 375, 874, doi: [10.1126/science.abl4679](https://doi.org/10.1126/science.abl4679)
- Rappaport, S., Joss, P. C., & Webbink, R. F. 1982, *ApJ*, 254, 616, doi: [10.1086/159772](https://doi.org/10.1086/159772)
- Schlafly, E. F., & Finkbeiner, D. P. 2011, *ApJ*, 737, 103, doi: [10.1088/0004-637X/737/2/103](https://doi.org/10.1088/0004-637X/737/2/103)
- Schlegel, D. J., Finkbeiner, D. P., & Davis, M. 1998, *ApJ*, 500, 525, doi: [10.1086/305772](https://doi.org/10.1086/305772)
- Shidatsu, M., Nakahira, S., Murata, K. L., et al. 2019, *ApJ*, 874, 183, doi: [10.3847/1538-4357/ab09ff](https://doi.org/10.3847/1538-4357/ab09ff)
- Straižys, V. 1992, *Multicolor stellar photometry* (Tucson: Pachart Pub. House)
- Torres, M. A. P., Casares, J., Jiménez-Ibarra, F., et al. 2020, *ApJL*, 893, L37, doi: [10.3847/2041-8213/ab863a](https://doi.org/10.3847/2041-8213/ab863a)
- . 2019, *ApJL*, 882, L21, doi: [10.3847/2041-8213/ab39df](https://doi.org/10.3847/2041-8213/ab39df)
- Tucker, M. A., Shappee, B. J., Holoiën, T. W. S., et al. 2018, *ApJL*, 867, L9, doi: [10.3847/2041-8213/aae88a](https://doi.org/10.3847/2041-8213/aae88a)
- Verbunt, F. 1993, *ARA&A*, 31, 93, doi: [10.1146/annurev.aa.31.090193.000521](https://doi.org/10.1146/annurev.aa.31.090193.000521)
- Wang, J., Mastroserio, G., Kara, E., et al. 2021, *ApJL*, 910, L3, doi: [10.3847/2041-8213/abec79](https://doi.org/10.3847/2041-8213/abec79)
- Wood, C. M., Miller-Jones, J. C. A., Homan, J., et al. 2021, *MNRAS*, 505, 3393, doi: [10.1093/mnras/stab1479](https://doi.org/10.1093/mnras/stab1479)
- Zdziarski, A. A., Dziełak, M. A., De Marco, B., Szanecki, M., & Niedźwiecki, A. 2021, *ApJL*, 909, L9, doi: [10.3847/2041-8213/abe7ef](https://doi.org/10.3847/2041-8213/abe7ef)
- Zdziarski, A. A., Ziółkowski, J., & Mikołajewska, J. 2019, *MNRAS*, 488, 1026, doi: [10.1093/mnras/stz1787](https://doi.org/10.1093/mnras/stz1787)
- Ziółkowski, J. 2005, *MNRAS*, 358, 851, doi: [10.1111/j.1365-2966.2005.08796.x](https://doi.org/10.1111/j.1365-2966.2005.08796.x)
- Ziółkowski, J., & Zdziarski, A. A. 2017, *MNRAS*, 469, 3315, doi: [10.1093/mnras/stx1084](https://doi.org/10.1093/mnras/stx1084)
- . 2018, *MNRAS*, 480, 1580, doi: [10.1093/mnras/sty1948](https://doi.org/10.1093/mnras/sty1948)